Journal of Radioanalytical and Nuclear Chemistry (2018) 318:1119–1129
https://doi.org/10.1007/s10967-018-6163-z

Recovery of U(VI) from simulated wastewater with thermally modified palygorskite beads

Aixia Zhou[1] · Jinsheng Wang[1]

Received: 6 June 2018 / Published online: 28 August 2018

Abstract

Natural palygorskite has a restricted adsorption capacity. The uranium ion removal ability of thermally modified palygorskite (T/Pal) beads from simulated wastewater was evaluated. T/Pal and T/Pal beads were characterized by several analytical methods. The influence of pH, contact time, temperature, and initial U(VI) concentration on the adsorption of T/Pal beads was investigated. The adsorption efficiency of U(VI) by T/Pal beads reached 99% within 20 min and the adsorption capacity was 20.23 mg g^{-1} at 313 K. The reusability of T/Pal bead was demonstrated by five sorption–desorption cycles. T/Pal beads are promising, economical adsorbents for the recovery of U(VI), and for radioactive wastewater decontamination.

Keywords Palygorskite(Pal) · Sodium alginate · Adsorption · Uranium · Wastewater

Introduction

Radioactive waste results from the nuclear power, iatrical, and military schemes as well as industrial activities [1–3]. Radioactive waste poses a serious threat to the environment and human health [3–5]. U(VI) is the primary heavy metal contaminant in wastewater and groundwater around disposal sites. The recovery of U(VI) ions from wastewater attracted great attention due to their long half-life, high toxicity, and regeneration as an energy resource [1, 5, 6]. Several adsorbents have been employed to recover the radioactive contaminants from wastewater, including multilayer titanate nanotubes [7], chelating weak base resin [8], hydroxide/graphene hybrid material [9], functionalized magnetic mesoporous silica nanoparticles [10], hematite [11], chitosan beads [12], biochar [13], and bituminous shale [14]. However, the above adsorbents, due to complex manufacturing processes, expensive costs, secondary pollution and poor persistence, are unsuited to application in practical engineering.

Palygorskite (Pal) is a natural non-metallic clay mineral with large superficial area, multiaperture structure and great cation exchange capacity [15–19]. Hence, Pal has excellent absorbability of metal ions, such as Cu, Ca, Sb, U and Th [20–22]. The heat treatment technique can modify the structure of palygorskite, removing water, hydroxyl groups, and impurities at different temperatures [3, 23, 24]. The activity of palygorskite was improved [25–27]. Thermally treated palygorskite at different temperatures was superior to untreated palygorskite in enhancing the wear resistance of Polytetra fluoroethene (PTFE) [24]. Thermal treatment methods change the inner surface of the tunnel-like structure of Pal, improving its surface area to over 300 m^2/g, as well as its adsorption capacity [29, 30]. However, the treated palygorskite powders were difficult to separate from wastewater, and filtration or high-pressure filter methods would increase costs in practical applications. Therefore, it is imperative to seek a method to easily separate palygorskite from wastewater.

Sodium alginate (NaAlg), an anionic natural macromolecule, is comprised of β-D-mannuronic (M units) and α-L-guluronic (G units) by 1–4 linkages [27]. NaAlg, a natural polysaccharide, is renewable, abundant source, non-toxic, water-soluble, biodegradable and biocompatible. Because of these advantages, NaAlg has attracted

Electronic supplementary material The online version of this article (https://doi.org/10.1007/s10967-018-6163-z) contains supplementary material, which is available to authorized users.

✉ Aixia Zhou
zhouaixia2010@sina.com

[1] College of Water Sciences, Beijing Normal University, Beijing 100088, China

significant attention in the environmental fields. Wang et al. [28] applied alginate-based Pal foams as efficient adsorbents for the decontamination of heavy metal-polluted wastewater. Shao et al. [29] utilized engineered NaAlg-based beads to adsorb toxic metal ions and cationic dyes. However, the study of the application of sodium alginate-palygorskite to U(VI) removal is rare.

Herein, the U(VI) adsorption behavior of sodium alginate-thermally treated palygorskite was studied. The purpose of this research was (1) to synthesize sodium alginate-thermally treated palygorskite beads and to study their characteristics using SEM (Scanning Electron Microscope), EDS (Energy Disperse Spectroscopy), TEM (Energy Disperse Spectroscopy), XRD (X-Ray Diffraction) analysis and other physical and chemical analysis methods; (2) to explore the adsorption theory of U(VI) ion adsorption by T/Pal beads; (3) to identify the dynamic conditions of U(VI) ion adsorption on T/Pal beads by simulated columns.

Experimental

Materials

Pal was gained from Xuyi, Jiangsu Province, while the $UO_2(NO_3)_2{\cdot}6H_2O$ and other chemicals were purchased from Sinopharm Chemical Reagent Beijing Co. Ltd. (Beijing, China). 1.0 g L^{-1} of U(VI) stock solution was produced by solubilizing $UO_2(NO_3)_2{\cdot}6H_2O$ powder in deionized water.

The synthesis of modified Pal

10 g of palygorskite was pulverized and sieved through a 100 mesh sieve. The pulverized palygorskite was placed in a 400 mL beaker, with deionized water and 0.3 g of $(NaPO_3)_6$ as dispersants. The mixed solution was stirred for 30 min using a magnetic stirring apparatus (Shanghai Zhenrong Science Instrument Co. Ltd) and dispersed for 1 h using ultrasonic instrumentation (Hangzhou Farrant Ultrasonic Technology Co. Ltd.). The solution was centrifuged for 15 min at 3300 r min^{-1} and dried for 3 h in an oven (65 °C). The dried palygorskite was pulverized, sieved through another 100 mesh sieve, and sealed for use.

The purified palygorskite (T/Pal) was calcinated at the desired temperature (100, 200, 300, 400 °C) in a muffle furnace and sealed in a hermetic bag for the following experiments, after cooling. The T/Pal powder was mixed with sodium alga acid and added dropwise into the $CaCl_2$ solution at a constant velocity to form the T/Pal beads. The beads were dried for 2 h at 110 °C and stored in sealed bags until further use.

Batch experiments

A fixed number of beads (0.05 g) was added to vials with 10 mL U(VI) diluted solution (10–100 mg L^{-1}). The vials were shaken at 150 rpm at 25 °C for a set time(10, 20, 30, 60, 180, 300 min). The supernatant was sampled at a regular interval and the concentration of U(VI) was measured by spectrophotometry (WGJ-III, Daji Photoelectric Instrument Co., Ltd, Hangzhou, China) after filtering through 0.45 μm microfiltration membranes. The adsorption efficiency (Adsorption, %) and adsorption capacity (q_t, mg g^{-1}) were obtained from Eqs. (1) and (2), respectively.

$$q_t = \frac{V \times (C_0 - C_t)}{m} \quad (1)$$

$$\text{Adsorption}(\%) = \frac{(C_0 - C_t)}{C_0} \times 100\% \quad (2)$$

where C_0 (mg L^{-1}) is the initial concentration, C_t (mg L^{-1}) is the residual U(VI) concentration, m (g) is the weight of the beads, and V (L) is the volume of the adsorption system.

The initial U(VI) concentrations were set to 10, 20, 50, 100 mg L^{-1}, and the pH of reaction solution was set at 2, 3, 4, 5, 7, 9 and 11 to inspect the influence of the initial concentration and pH on the adsorption of U(VI) ions by the T/Pal beads. The pH of system was adjusted by NaOH and HNO_3. All experiments were repeated three times.

Characteristics of the sorbent

The modified Pal was characterized by SEM–EDS (Hitachi S-4800/EX-350, Suzhou, China)and TEM (H-7650, Hitachi Company, Japan) to analyze the size and morphology of the adsorbents in this work. The structure of the modified Pal was analyzed by XRD (X' Pert PRO MPD, PANalytical B. V., Netherlands). The TG–DTA of Pal was analyzed by thermo gravimetric analyzer (TGA-101, Nanjing Dazhan Institute of Electromechanical Technology, China).

Sorption–desorption experiments

Several sorption–desorption cycles were performed at pH 6. To maintain the same experimental conditions, two mother liquids were prepared: (1) a fixed concentration of U(VI) (100 mg L^{-1}) at pH 6. (2) The eluent agent (0.1 M HCl solution at pH 1). After each desorption procedure, the T/Pal beads were washed with water to remove the redundant eluent on the surface of the T/Pal beads. The efficiency of the elution was determined by calculating the ratio of desorbed mass to sorbed mass.

Dynamic column

The glass columns (inner diameter: 2.1 cm) were filled with the T/Pal beads up to a height of 6.5 cm. The pore volume of the column was calculated by full water test. The U(VI) solution (10 mg L^{-1}) was delivered by a peristaltic pump (0.016 L h^{-1}) at 25 °C in the up-flow mode. After dynamic adsorption experiments, the saturated column was washed downwards using the eluent solution.

The breakthrough curve represents the behavior of U(VI) adsorption onto the sorbents; it is plotted as the ratio of effluent concentration to inlet concentration (C_t/C_0) as a function of the experimental time t (the influent/pore volume of the column, called pore volume, PV).

Results and discussions

Pal characteristics

The characterization of the T/Pal beads is shown in Fig. 1. As can be seen from Fig. 1a, b, a rod-like shape, 200–1000 nm long was observed. Compared with natural Pal, the rod structure of the T/Pal was clearer. At high temperatures, low-stability impurities are eliminated from the structure, making the angles of the outline of T/Pal clearer [31, 32]. According to the crystal structure of Pal, water exists in five states in Pal, which increase in stability in the following order: surface adsorption water, zeolitic water, adsorption water, crystal water and bound water [19, 33]. Figure 1c shows the TG (Thermogravimetry) and DTA (Differential Thermal Analysis) curves for Pal in an inert environment with a temperature of 20–800 °C. The zeolitic water existed in the voids of the Pal structure and the water adsorbed on the outer surfaces was totally removed above 200 °C, resulting in a mass loss of 9.1%. From 230 °C to 481 °C, the crystal water was desorbed. Due to the crystal water desorption, the Pal structure folds. There is one endothermic peak at about 450–500 °C for Pal. In the high-temperature region (> 600 °C) an endothermic effect (at about 800 °C) is immediately followed by an exothermic maximum. According to the XRD results (Fig. 1d), at 400 °C, the characteristic diffraction peaks (110), (200), (040), (400) and (161) of Pal were weakened. The higher temperature (> 400 °C) treatment would make the structure of Pal collapse, and lose amount of adsorption sites, while the lower temperature(< 400 °C) treatment would not thoroughly clean the impurities in the channel of Pal. Moreover, the adsorption of U(VI) ions by T/Pal treated at 400 °C was best (Fig. S1). Thus, 400 °C was the optimum processing temperature.

Figure 2 showed that the inner diameter of the T/Pal bead was about 1.53–2.35 mm, and the surface of the bead was irregular and flocculent. The surface of the T/Pal bead

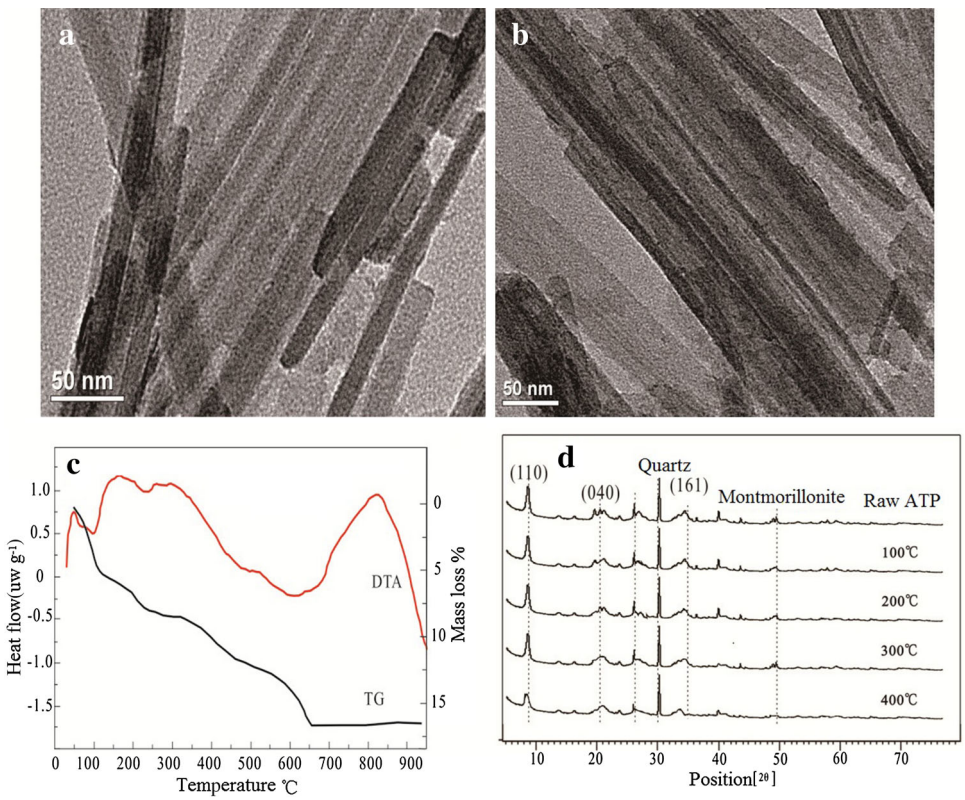

Fig. 1 The characterization of T/Pal (**a** and **b** TEM of Pal and T/Pal; **c** TG–DTA results; **d** XRD patterns)

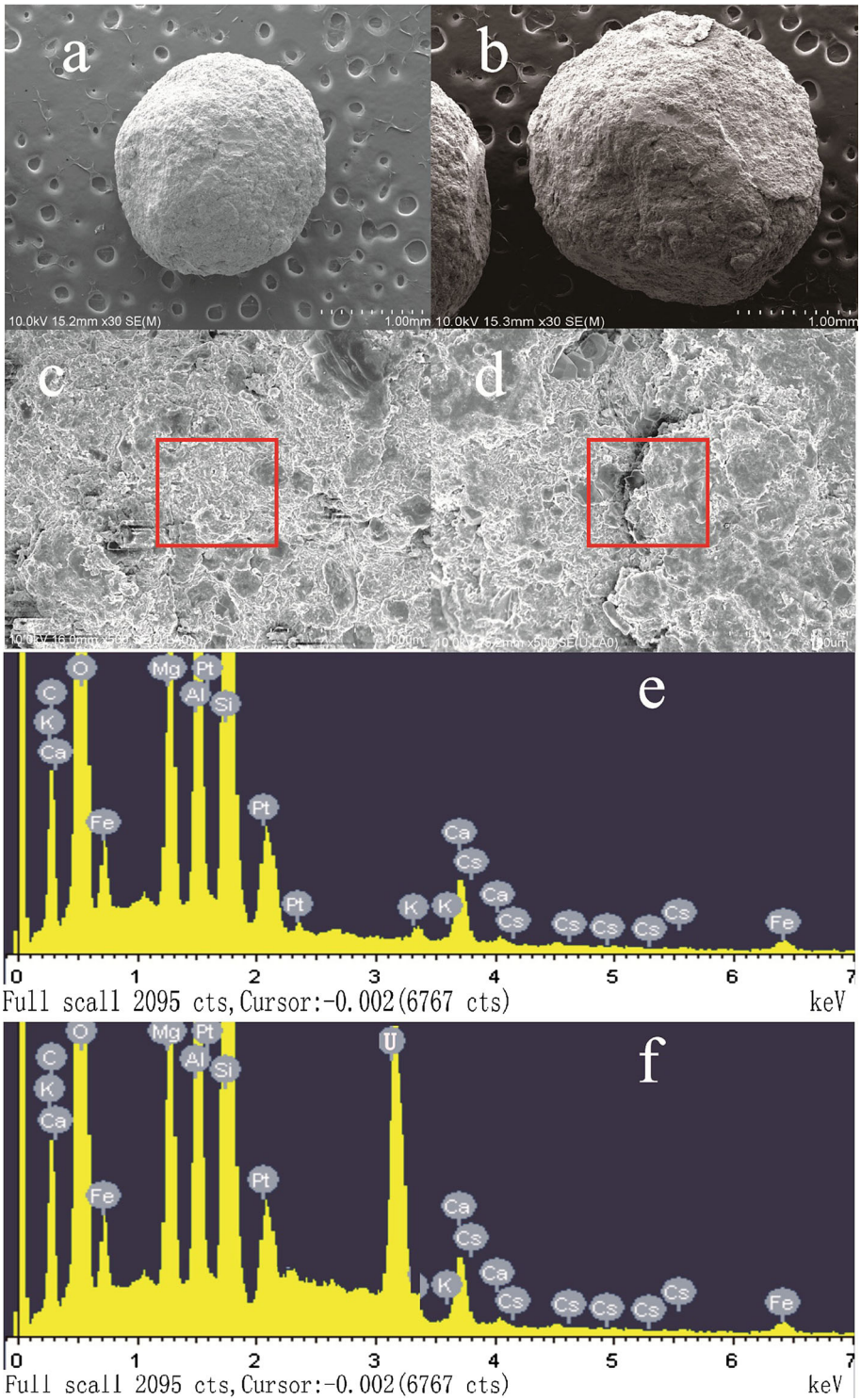

Fig. 2 The SEM and EDS images of T/Pal beads (**a**, **c** and **e** represent the data of the T/Pal beads before adsorption; **b**, **d** and **f** represent the data of the T/Pal beads after adsorption. The red box represents the location of the energy spectrum tests). (Color figure online)

was slightly changed before and after the adsorption of U(VI) ions (Fig. 2a and b). Comparing Fig. 2e and f, it is clear that the EDS results show that U(VI) ions exactly adsorbed onto the T/Pal beads.

Impacts of contact time

Figure 3a showed that the initial U(VI) adsorption rate onto T/Pal was more rapid at 313 K, and within 10 min the adsorption efficiency of U(VI) ions reached 90%,

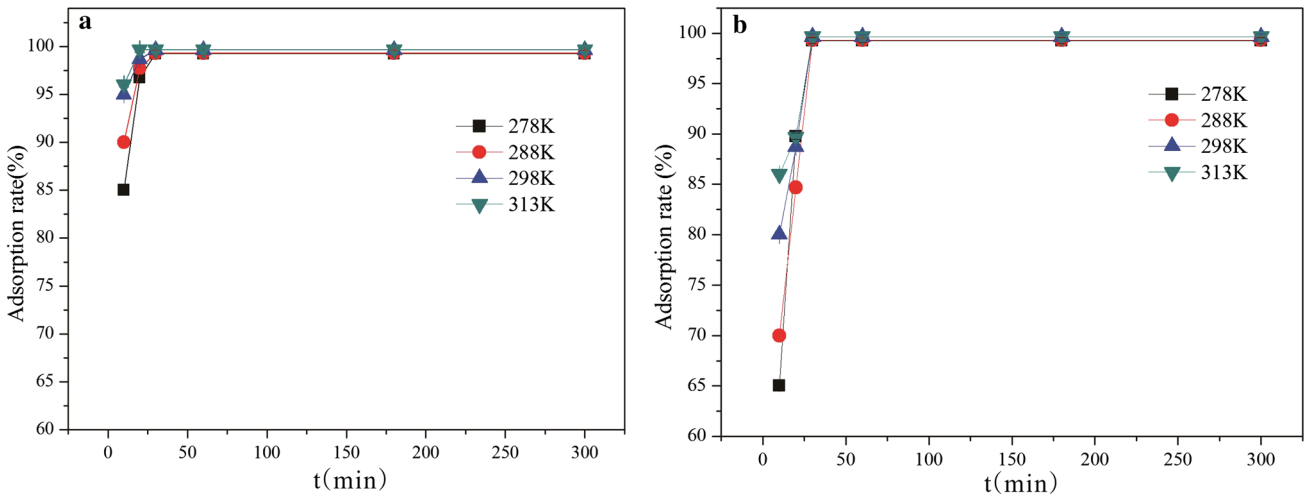

Fig. 3 The impact of contact time on U(VI) ion sorption by **a** T/Pal and **b** T/Pal beads

evidencing the rapid adsorption capacity of T/Pal. Although it was hypothesized that the adsorption of U(VI) ions by T/Pal beads was endothermal, the adsorption efficiency at 278 K remained close to 100%. The rapid adsorption was ascribed to the external physical adsorption and chemical adsorption between the U(VI) ions and the active groups on the T/Pal beads [34, 35,36]. In Fig. 3b the U(VI) adsorption onto the T/Pal beads was a little slower, but within 20 min the adsorption efficiency reached 99%. Due to the greater surface area of the T/Pal powder, there were more contact opportunities with U(VI) ions compared to T/Pal beads. The adsorption of U(VI) ions onto the T/Pal beads was also a rapid process.

Impacts of pH

The pH of the water could influence the surface charge of the adsorbent, the form of the metal, and the external sorption sites. Figure 4 indicates the influence of pH on U(VI) ion adsorption by T/Pal beads. The sorption of U(VI) ions on T/Pal was strongly influenced by pH of water (Fig. 4). The adsorption efficiency increased rapidly from pH 1 to pH 7, reaching the maximum at pH 7, and then declined with further increases in pH. However, the T/Pal beads were able to buffer the solution pH better than the powder. The adsorption rate of these beads reached more than 90% at pH 4, possibly due to the electrostatic attraction between the U(VI) ions and the electronegative groups ($-COO^-$ and $-SO_3^-$) on the T/Pal beads. The T/Pal beads were able to adapt to a broad pH range, and maintained a high adsorption rate and stability during the treatment of U(VI) polluted environments [31].

The adsorption of U(VI) ions onto the T/Pal beads could be explained by electrostatic binding. The scatter model of U(VI) ions in water was counted by Visual MINTEQ ver.

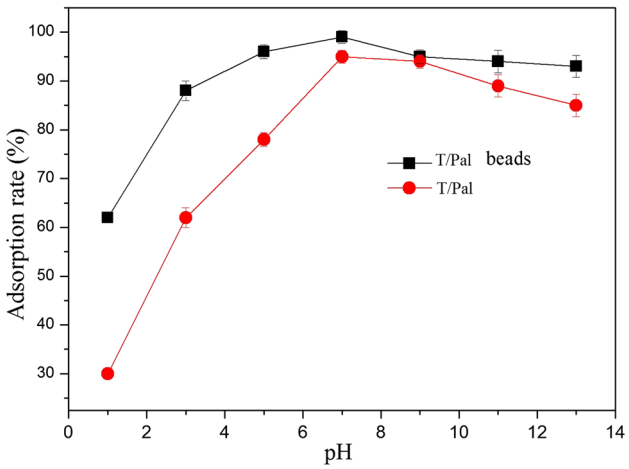

Fig. 4 Impacts of pH on U(VI) ion adsorption by T/Pal and T/Pal beads

3.0 (Fig. 5a); the main species of U(VI) ions at pH < 4.0 was UO_2^{2+}, whereas the hydrated U(VI) ion forms, such as $UO_2(OH)_3^-$, $UO_2(OH)_4^{2-}$, appeared during pH 5.0–8.0. When the pH exceeded 8.0, more electronegative forms, such as $(UO_2)_3(OH)_7^-$, occurred. The isoelectric point of T/Pal was 7.26, while the net surface charge of the T/Pal beads was positive at pH < 5.0. Due to the repulsion between the surface of the T/Pal beads and UO_2^{2+}, the adsorption of U(VI) onto the T/Pal beads became negative with the decline of UO_2^{2+}. The most rapid adsorption between U(VI) and T/Pal beads was at 5.0 < pH < 7.26, due to the attraction between the positively charged T/Pal surface sites and the electronegative U(VI) ions. Nevertheless, at pH > 7.26, adsorption declined due to the repulsion between the electronegative T/Pal adsorption sites and the negatively charged U(VI) forms. These anions

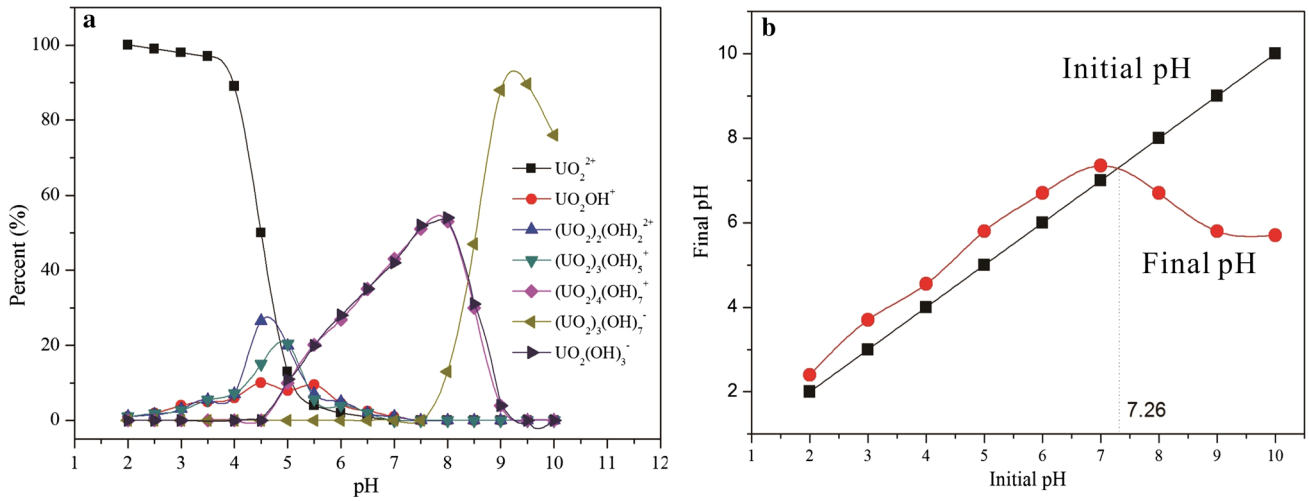

Fig. 5 The impacts of pH on the metal forms (**a**) and the surface charges of T/Pal (**b**)

were known for their low sorption affinity and their affinity for forming clathrates with CO_3^{2-} or HCO_3^-, so the U(VI) adsorption remained high.

Adsorption kinetics

Kinetic models [37, 38, 39, 40] (pseudo-first-order, pseudo-second-order and intra-particle diffusion models) were applied to fit the actual data of U(VI) ion sorption onto T/Pal beads. The expressions used are shown in Eqs. (3)–(5):

$$\ln(q_{e1} - q_t) = \ln q_{e1} - k_1 t \tag{3}$$

$$\frac{t}{q_t} = \frac{1}{k_2 q_{e2}^2} + \frac{t}{q_{e2}} \tag{4}$$

$$q_t = k_i t^{1/2} + C \tag{5}$$

where q_t (mg g^{-1}) is the U(VI) adsorption capacity at time t (min), q_e (mg g^{-1}) is the U(VI) adsorption capacity when the adsorption reaches equilibrium, k_1 (h^{-1}) is the rate constant of the pseudo-first-order model, k_2 (g mg^{-1} h^{-1}) is the rate constant of the second-order model. k_i (mg g^{-1} $h^{-0.5}$) is the rate constant of the intraparticle transport model, and C is a constant. The pseudo-first and pseudo-second order models are macroscopic models, and are usually applied to describe the adsorption process [41, 42]. The construction of intra-particle diffusion is the rate-determining step [39].

The plots of the pseudo-first-order model, pseudo-second-order model and intra-particle diffusion kinetics model for the above equations are shown in Fig. 6, and the parameters used in the linear equations are given in Table 1. As can be seen from the correlation coefficients (R^2), the adsorption process was best described by the pseudo second-order model.

As the sorption of U(VI) to the T/Pal beads was best described by the pseudo-second-order model, one of the adsorption mechanisms was likely exchange of electrons between the adsorbent and adsorbate [40], and the rate-controlling step of U(VI) ion sorption onto the T/Pal beads was chemisorption, rather than mass transport. The adsorption capacity and rates could also be calculated by Eqs. (3)–(5); the adsorption capacity of the U(VI) ions obtained by the pseudo-second-order kinetic equation was in total agreement with the experimental data. More importantly, the adsorption of U(VI) ions onto the T/Pal beads was rapid. The adsorption rate was up to 10.23 g mg^{-1} h^{-1} at an initial concentration of 100 mg L^{-1}. The adsorption of U(VI) ions onto the T/Pal beads took advantage of a preferable adsorption capacity and adsorption rate.

The q_t versus $t^{1/2}$ plot would pass through the origin if intra-particle diffusion was the only rate-controlling step. As shown in Fig. 6c, the plots were not linear and were comprised of two stages. The adsorption rate was rapid during stage I and up to 34.52 g mg^{-1} $h^{-0.5}$ at an initial concentration 100 mg L^{-1}. The first stage was ascribed to the diffusion of U(VI) ions from the solution to the surface of the T/Pal beads, while the second stage was due to the intra-particle diffusion of U(VI) ions into the interior of the T/Pal beads.

Equilibrium adsorption

The sorption isotherms of U(VI) ions onto T/Pal beads at 278, 288, 298 and 313 K are shown in Fig. 7. The adsorption capacity is the highest at 313 K and the lowest

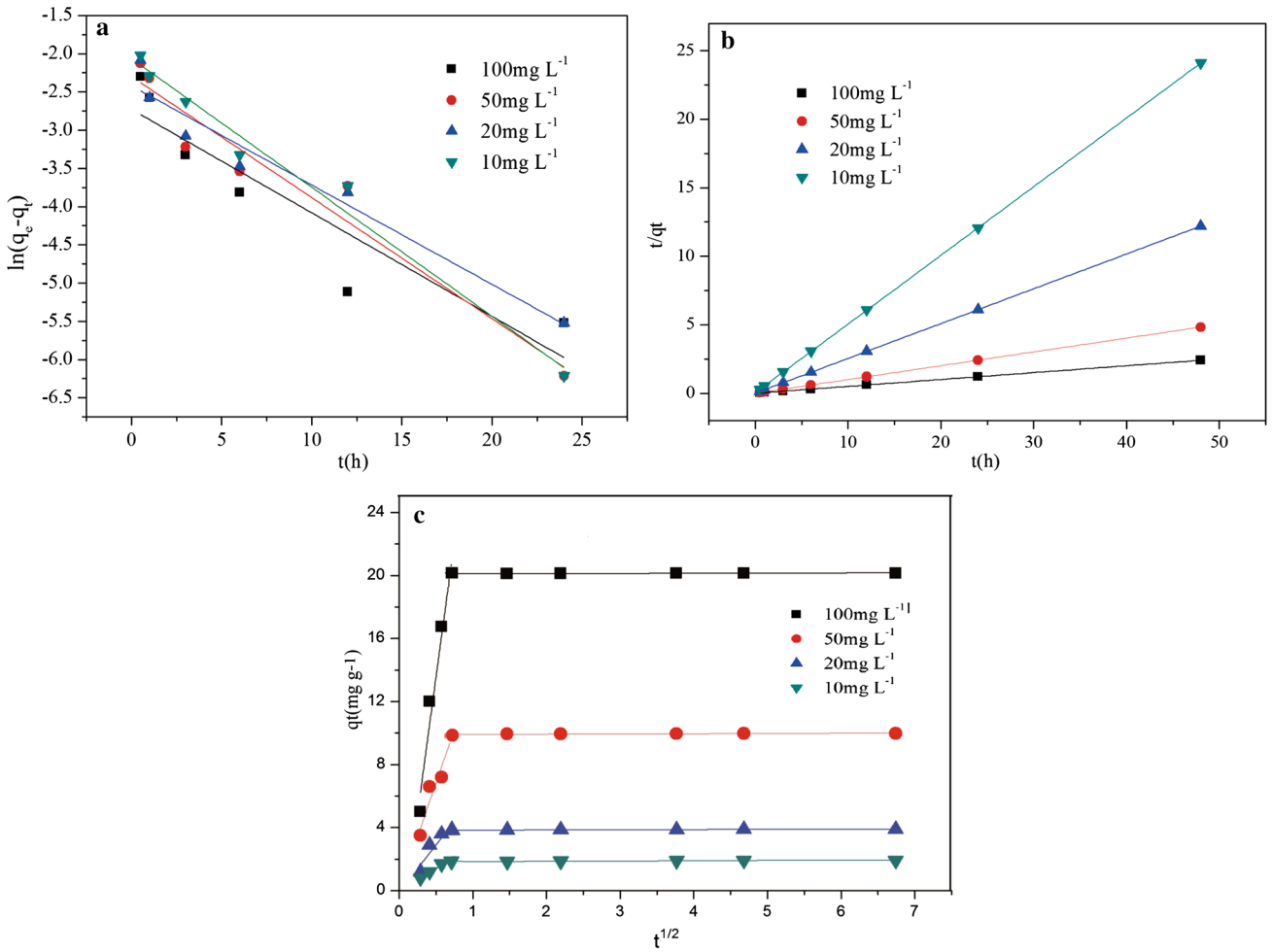

Fig. 6 Kinetic plots (**a** Pseudo-first-order kinetic; **b** Pseudo-second-order kinetic; **c** Intra-particle diffusion kinetics)

Table 1 Parameters of kinetic equation for the adsorption of U(VI) ions on T/Pal beads

Initial concentration	Pseudo-first-order				Pseudo-second-order		
	q_e	q_{e1}	k (h^{-1})	R^2	q_{e2}	k (mg g^{-1} h^{-1})	R^2
100 mg L^{-1}	19.94	0.07	0.14	0.8227	19.93	10.23	0.9999
50 mg L^{-1}	9.93	0.10	0.16	0.9307	9.94	6.80	0.9999
20 mg L^{-1}	3.94	0.09	0.13	0.9420	3.94	6.70	0.9999
10 mg L^{-1}	1.99	0.13	0.17	0.9763	2.00	5.42	0.9999

	k_1 (mg g^{-1} $h^{-0.5}$)	C_1	R_1^2	k_2 (mg g^{-1} $h^{-0.5}$)	C_2	R_2^2
Intra-particle diffusion						
100 mg L^{-1}	34.52	− 3.71	0.9420	0.010	19.87	0.6372
50 mg L^{-1}	13.58	0.05	0.8834	0.014	9.85	0.6268
20 mg L^{-1}	5.95	− 0.07	0.7742	0.012	3.86	0.8039
10 mg L^{-1}	2.60	0.10	0.9558	0.016	1.90	0.7818

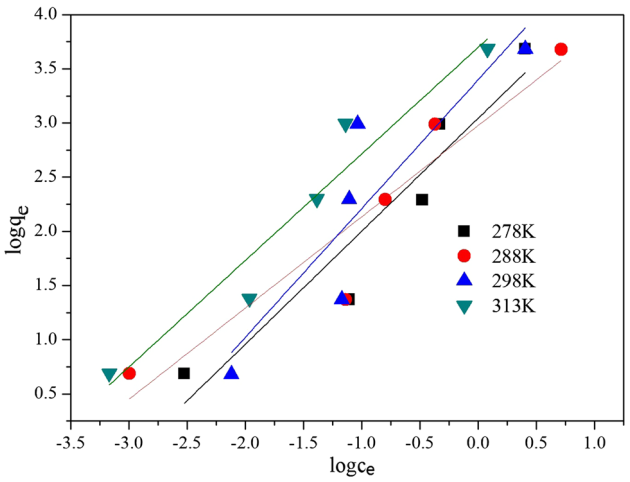

Fig. 7 Freundlich isotherm of U(VI) adsorption onto T/Pal beads

at 278 K, meaning U(VI) ions adsorption onto T/Pal beads is endothermic.

The Langmuir and Freundlich equations [45, 46], which describe the adsorption process, are shown in Eqs. (6) and (7).

$$\frac{C_e}{q_e} = \frac{1}{q_0 b} + \frac{C_e}{q_0} \tag{6}$$

$$\log q_e = \log K_f + \frac{1}{n}\log C_e \tag{7}$$

where C_e is the U(VI) ion concentration at equilibrium (mg L^{-1}), q_e is the U(VI) adsorption capacity (mg g^{-1}) at equilibrium, q_0 is the saturated monolayer adsorption capacity (mg g^{-1}), b is the Langmuir constant (L mg^{-1}), K_f is the Freundlich constant, relates to the adsorption capacity [(mg g^{-1}) (L $mg^{-1})^{1/n}$]. Finally, n represents the intensity of adsorption. It is more suitable to describe multilayer adsorption and non-ideal adsorption on heterogeneous surfaces of adsorbents by the Freundlich model. The parameters obtained from the two equilibrium models are shown in Table 2.

Column adsorption of U(VI)

The Thomas model equation is usually applied to depict the theoretical property of the adsorbent column performance, due to its uncomplicated and fairly precise method in predicting breakthrough curves. The model expression is shown in the following equation [43]:

$$\frac{C_t}{C_0} = \frac{1}{1 + \exp[K_T(q_T m - C_0 V)/Q]} \tag{8}$$

where K_T is the rate constant (L h^{-1} mg^{-1}), m is the weight of the sorbent (g), Q is the flow rate (L h^{-1}), C_t is the concentration at t (mg g^{-1}), and q_T is the adsorption capacity (mg g^{-1}).

It was important to apply the continuous fixed system to measure the feasibility of the adsorbent [44]. The adsorption columns were frequently used to evaluate the adsorption efficiency in almost real-world conditions [45]. Figure 8 shows the sorption and desorption of the columns, in which the experimental data fitted well to the Thomas model equation (Fig. 8a) (R^2 = 0.9983). The estimated q_T was 1.97 mg g^{-1}, which was close to the actual measured value (1.89 mg g^{-1}) (Table 3). The elution of the columns revealed that the U(VI) ions could be recovered from the loaded T/Pal beads. Figure 8b showed that only 0.12 L of eluent was required to regenerate the adsorption column, which indicated the feasibility of using T/Pal beads as sorbent to recover U(VI) ions from industrial wastewater.

A good sorbent must be recyclable to be used in large-scale applications. The reusability of T/Pal beads was demonstrated by five sorption–desorption cycles. The results are shown in Table 4. The sorption rate of U(VI) tends to decrease after repeated cycles, but it remained higher than 80% after 5 cycles.

The comparison with other adsorbents

As can be seen from Table 5, the adsorption capacity of U(VI) on T/Pal beads was higher than that of some geological sorbents (Hematite, Dunite, Clinoptilolite, Kaolin) [11, 46–48], while lower than that of some high polymer material adsorbents (Magnetic mesoporous silica nanoparticles, Superparamagnetic polymer microspheres and Multilayer titanate nanotubes) [7, 10, 49]. However, these high polymer material adsorbents are unsuited to application in practical engineering, due to the complex

Table 2 Equilibrium adsorption parameters

Temperature	Langmuir		Freundlich		
	q_m(mg g^{-1})	R^2	K_f (mg g^{-1}) (L $mg^{-1})^{1/n}$	n	R^2
278 K	19.856	0.8971	17.30	1.09	0.9110
288 K	19.862	0.8644	19.62	1.19	0.8721
298 K	19.939	0.7233	29.93	0.84	0.8293
313 K	20.230	0.9211	40.39	1.02	0.9250

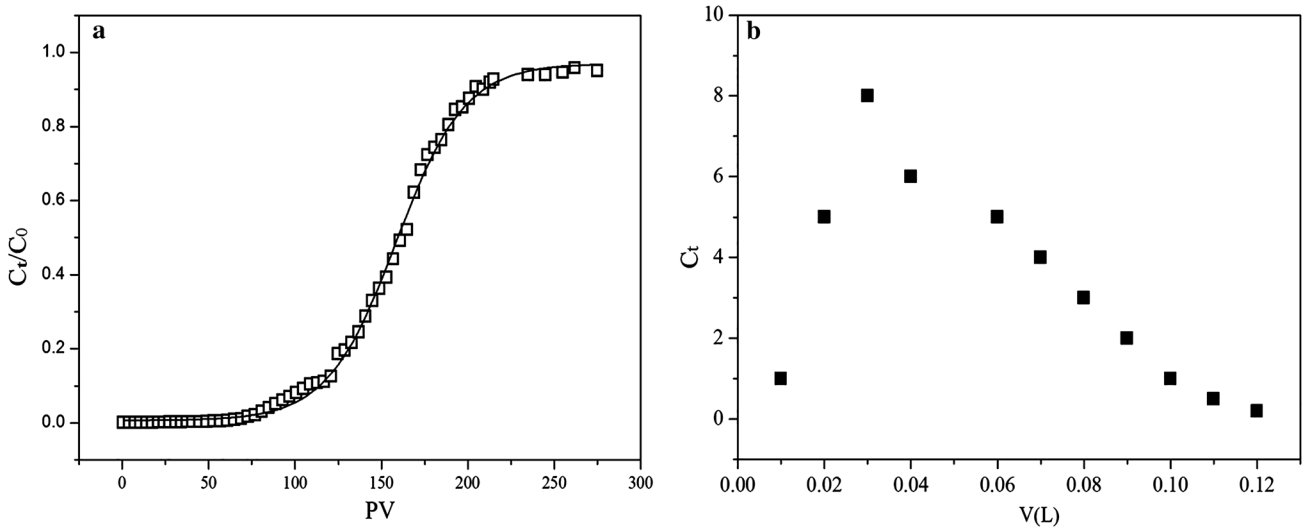

Fig. 8 The results of adsorption column (**a** the breakthrough curve; **b** the elution curve)

Table 3 Adsorption column parameters using T/Pal beads

q_{exp} (mg g^{-1})	Experimental			Thomas parameters		
	Sorption efficiency (%)	q_{BP}	PV	q_T (mg g^{-1})	K_T (L h^{-1} mg^{-1})	R^2
1.89	78	1.4	275	1.97	6.5×10^{-2}	0.9983

Table 4 The sorption and desorption parameters

1st Cycle		2nd Cycle		3rd Cycle		4th Cycle		5th Cycle	
Sorption efficiency (%)	Elution (%)	Sorption efficiency (%)	Elution (%)	Sorption efficiency (%)	Elution (%)	Sorption efficiency (%)	Elution (%)	Sorption efficiency (%)	Elution (%)
96.9	82.3	95.3	86.7	92.7	90.3	90.3	91.2	86.4	95.3

Table 5 The comparison of adsorption capacity of U(VI) with other adsorbents

Adsorbents	q_{max} (mg g^{-1})	References
T/Pal beads	20.23	This work
Hematite	5.59	[11]
Dunite	16.66	[46]
Clinoptilolite	8.09	[47]
Kaolin	4.76	[48]
Magnetic mesoporous silica nanoparticles	133.00	[10]
Superparamagnetic polymer microspheres	200.50	[49]
Multilayer titanate nanotubes	300.00	[7]

manufacturing processes, expensive costs, secondary pollution and so on. Thus, T/Pal beads can be as a promising candidate for the recovery of U(VI) from aqueous solution due to its low-cost, sustainable, and efficient features.

Conclusion

The T/Pal beads prepared in this study have the good mechanical properties and showed desirable U(VI) adsorption abilities. The large sorption capacity, good

regeneration property and recyclability can decrease the treatment cost of U(VI) polluted water. T/Pal beads will be an excellent adsorbent for the recovery of U(VI) ions during the treatment of radioactive wastewater and nuclear waste management.

Acknowledgements The authors are grateful for a research grant provided by the National Natural Science Foundation of China (No. 41372233). We are grateful to the students who assisted us with this project and the anonymous reviewers of the manuscript.

References

1. Amaral JCBS, Morais CA (2010) Thorium and uranium extraction from rare earth elements in monazite sulfuric acid liquor through solvent extraction. Miner Eng 23:498–503. https://doi.org/10.1016/j.mineng.2010.01.003
2. Boy-Roura M, Mas-Pla J, Petrovic M et al (2018) Towards the understanding of antibiotic occurrence and transport in groundwater: findings from the Baix Fluvià alluvial aquifer (NE Catalonia, Spain). Sci Total Environ 612:1387–1406. https://doi.org/10.1016/J.SCITOTENV.2017.09.012
3. Zhao G, Wen T, Yang X et al (2012) Preconcentration of U(vi) ions on few-layered graphene oxide nanosheets from aqueous solutions. Dalton Trans 41:6182. https://doi.org/10.1039/c2dt00054g
4. Li JQ, Le Gong L, Feng XF et al (2017) Direct extraction of U(VI) from alkaline solution and seawater via anion exchange by metal-organic framework. Chem Eng J 316:154–159. https://doi.org/10.1016/j.cej.2017.01.046
5. John AMS, Cattrall RW, Kolev SD (2010) Extraction of uranium(VI) from sulfate solutions using a polymer inclusion membrane containing di-(2-ethylhexyl) phosphoric acid. J Membr Sci 364:354–361. https://doi.org/10.1016/j.memsci.2010.08.039
6. Miretzky P, Cirelli AF (2010) Cr(VI) and Cr(III) removal from aqueous solution by raw and modified lignocellulosic materials: a review. J Hazard Mater 180:1–19
7. Liu W, Zhao X, Wang T et al (2016) Adsorption of U(VI) by multilayer titanate nanotubes: effects of inorganic cations, carbonate and natural organic matter. Chem Eng J 286:427–435. https://doi.org/10.1016/j.cej.2015.10.094
8. Ogden MD, Moon EM, Wilson A et al (2017) Corrigendum to "Application of chelating weak base resin Dowex M4195 to the recovery of uranium from mixed sulfate/chloride media" [Chem. Eng. J. 317 (2017) 80–89]. Chem Eng J 324:414. https://doi.org/10.1016/J.CEJ.2017.04.141
9. Tan L, Wang Y, Liu Q et al (2015) Enhanced adsorption of uranium (VI) using a three-dimensional layered double hydroxide/graphene hybrid material. Chem Eng J 259:752–760. https://doi.org/10.1016/J.CEJ.2014.08.015
10. Li D, Egodawatte S, Kaplan DI et al (2016) Functionalized magnetic mesoporous silica nanoparticles for U removal from low and high pH groundwater. J Hazard Mater 317:494–502. https://doi.org/10.1016/J.JHAZMAT.2016.05.093
11. Zhao D, Wang X, Yang S et al (2012) Impact of water quality parameters on the sorption of U(VI) onto hematite. J Environ Radioact 103:20–29. https://doi.org/10.1016/j.jenvrad.2011.08.010
12. Sohbatzadeh H, Keshtkar AR, Safdari J et al (2017) Insights into the biosorption mechanisms of U(VI) by chitosan bead containing bacterial cells: a supplementary approach using desorption eluents, chemical pretreatment and PIXE–RBS analyses. Chem Eng J 323:492–501. https://doi.org/10.1016/j.cej.2017.04.088
13. Ashry A, Bailey EH, Chenery SRN, Young SD (2016) Kinetic study of time-dependent fixation of UVIon biochar. J Hazard Mater 320:55–66. https://doi.org/10.1016/j.jhazmat.2016.08.002
14. Ortaboy S, Atun G (2014) Kinetics and equilibrium modeling of uranium(VI) sorption by bituminous shale from aqueous solution. Ann Nucl Energy 73:345–354. https://doi.org/10.1016/j.anucene.2014.07.003
15. Cheng W, Ding C, Sun Y, Wang X (2015) Fabrication of fungus/attapulgite composites and their removal of U(VI) from aqueous solution. Chem Eng J 269:1–8. https://doi.org/10.1016/J.CEJ.2015.01.096
16. Tang J, Mu B, Zong L, Wang A (2018) One-step synthesis of magnetic attapulgite/carbon supported NiFe-LDHs by hydrothermal process of spent bleaching earth for pollutants removal. J Clean Prod 172:673–685. https://doi.org/10.1016/J.JCLEPRO.2017.10.181
17. Wu W, Fan Q, Xu J et al (2007) Sorption-desorption of Th(IV) on attapulgite: effects of pH, ionic strength and temperature. Appl Radiat Isot 65:1108–1114. https://doi.org/10.1016/j.apradiso.2007.05.009
18. Liu P, Wang T (2007) Adsorption properties of hyperbranched aliphatic polyester grafted attapulgite towards heavy metal ions. J Hazard Mater 149:75–79. https://doi.org/10.1016/j.jhazmat.2007.03.048
19. Chen H, Zhao J, Zhong A, Jin Y (2011) Removal capacity and adsorption mechanism of heat-treated palygorskite clay for methylene blue. Chem Eng J 174:143–150. https://doi.org/10.1016/j.cej.2011.08.062
20. Gan F, Zhou J, Wang H et al (2009) Removal of phosphate from aqueous solution by thermally treated natural palygorskite. Water Res 43:2907–2915. https://doi.org/10.1016/j.watres.2009.03.051
21. Wang J, Chen D (2013) Mechanical properties of natural rubber nanocomposites filled with thermally treated attapulgite. J Nanomater. https://doi.org/10.1155/2013/496584
22. Biswas B, Sarkar B, Naidu R (2016) Influence of thermally modified palygorskite on the viability of polycyclic aromatic hydrocarbon-degrading bacteria. Appl Clay Sci 134:153–160. https://doi.org/10.1016/j.clay.2016.07.003
23. Chen H, Zhong A, Wu J et al (2012) Adsorption behaviors and mechanisms of methyl orange on heat-treated palygorskite clays. Ind Eng Chem Res 51:14026–14036. https://doi.org/10.1021/ie300702j
24. Lai SQ, Li TS, Liu XJ et al (2006) The tribological properties of PTFE filled with thermally treated nano-attapulgite. Tribol Int 39:541–547. https://doi.org/10.1016/j.triboint.2005.03.016
25. Yuhuan W, Jianqing W, Yu Z et al (2012) Study on adsorption thermodynamics and kinetics of thermal- modified attapulgite clay. https://doi.org/10.13475/j.fzxb.2012.05.010
26. Ye H, Chen F, Sheng Y et al (2006) Adsorption of phosphate from aqueous solution onto modified palygorskites. Sep Purif Technol 50:283–290. https://doi.org/10.1016/j.seppur.2005.12.004
27. Yang H, Wang W, Wang A (2012) A pH-sensitive biopolymer-based superabsorbent nanocomposite from sodium alginate and attapulgite: synthesis, characterization, and swelling behaviors. J Dispersion Sci Technol 33:1154–1162. https://doi.org/10.1080/01932691.2011.599244
28. Wang Y, Feng Y, Zhang XF et al (2018) Alginate-based attapulgite foams as efficient and recyclable adsorbents for the removal of heavy metals. J Colloid Interface Sci 514:190–198. https://doi.org/10.1016/j.jcis.2017.12.035
29. Shao Z, Huang X, Yang F et al (2018) Engineering sodium alginate-based cross-linked beads with high removal ability of

toxic metal ions and cationic dyes. Carbohyd Polym 187:85–93. https://doi.org/10.1016/j.carbpol.2018.01.092
30. Li X, Li F, Lu X et al (2018) Microwave hydrothermal synthesis of BiP1 − xVxO4/attapulgite nanocomposite with efficient photocatalytic performance for deep desulfurization. Powder Technol 327:467–475. https://doi.org/10.1016/j.powtec.2018.01.005
31. Xavier ALP, Adarme OFH, Furtado LM et al (2018) Modeling adsorption of copper(II), cobalt(II) and nickel(II) metal ions from aqueous solution onto a new carboxylated sugarcane bagasse. Part II: optimization of monocomponent fixed-bed column adsorption. J Colloid Interface Sci 516:431–445. https://doi.org/10.1016/j.jcis.2018.01.068
32. Ho YS (2004) Citation review of Lagergren kinetic rate equation on adsorption reactions. Scientometrics 59:171–177
33. Boukhelkhal A, Benkortbi O, Hamadache M et al (2016) Adsorptive removal of amoxicillin from wastewater using wheat grains: equilibrium, kinetic, thermodynamic studies and mass transfer. Desalin Water Treatment 57:27035–27047. https://doi.org/10.1080/19443994.2016.1166991
34. Zhu W, Liu Z, Chen L, Dong Y (2011) Sorption of uranium(VI) on Na-attapulgite as a function of contact time, solid content, pH, ionic strength, temperature and humic acid. J Radioanal Nucl Chem 289:781–788. https://doi.org/10.1007/s10967-011-1129-4
35. Fan HT, Sun W, Jiang B et al (2016) Adsorption of antimony(III) from aqueous solution by mercapto-functionalized silica-supported organic-inorganic hybrid sorbent: Mechanism insights. Chem Eng J 286:128–138. https://doi.org/10.1016/j.cej.2015.10.048
36. Lee S, Anderson PR, Bunker GB, Karanfil C (2004) EXAFS study of Zn sorption mechanisms on montmorillonite. Environ Sci Technol 38:5426–5432. https://doi.org/10.1021/es0350076
37. Choi J, Lee JY, Yang JS (2009) Biosorption of heavy metals and uranium by starfish and Pseudomonas putida. J Hazard Mater 161:157–162. https://doi.org/10.1016/j.jhazmat.2008.03.065
38. Jin X, Yu C, Li Y et al (2011) Preparation of novel nano-adsorbent based on organic-inorganic hybrid and their adsorption for heavy metals and organic pollutants presented in water environment. J Hazard Mater 186:1672–1680. https://doi.org/10.1016/j.jhazmat.2010.12.057
39. Wang J, Xue C, Wu Z et al (2012) Hollow micro-mesoporous carbon polyhedra produced by selective removal of skeletal scaffolds. Carbon 50:2546–2555. https://doi.org/10.1016/j.carbon.2012.02.003
40. Liu Y, Wang W, Wang A (2012) Effect of dry grinding on the microstructure of palygorskite and adsorption efficiency for methylene blue. Powder Technol 225:124–129. https://doi.org/10.1016/j.powtec.2012.03.049
41. Langmuir I (1918) The adsorption of gases on plane surfaces of glass, mica and platinum. J Am Chem Soc 40:1361–1403. https://doi.org/10.1021/ja02242a004
42. Freundlich HMF (1906) Über Die Absorption in Lösungen. Z Phys Chem 57:385–470. https://doi.org/10.1016/j.jclepro.2017.04.078
43. Chu KH (2010) Fixed bed sorption: setting the record straight on the Bohart-Adams and Thomas models. J Hazard Mater 177:1006–1012. https://doi.org/10.1016/j.jhazmat.2010.01.019
44. Abdolali A, Ngo HH, Guo W et al (2017) Application of a breakthrough biosorbent for removing heavy metals from synthetic and real wastewaters in a lab-scale continuous fixed-bed column. Biores Technol 229:78–87. https://doi.org/10.1016/j.biortech.2017.01.016
45. Demey H, Vincent T, Guibal E (2018) A novel algal-based sorbent for heavy metal removal. Chem Eng J 332:582–595. https://doi.org/10.1016/j.cej.2017.09.083
46. Demetriou A, Pashalidis I (2007) Adsorptionofhexavalenturani-umondunite. Glob Nest J 9:229–236
47. Kilincarslan A, Akyil S (2005) Uranium adsorption characteristic and thermodynamic behavior of clinoptilolite zeolite. J Radioanal Nucl Chem 264:541–548. https://doi.org/10.1007/s10967-005-0750-5
48. Wang G, Wang X, Chai X et al (2010) Adsorption of uranium (VI) from aqueous solution on calcined and acid-activated kaolin. Appl Clay Sci 47:448–451. https://doi.org/10.1016/j.clay.2009.11.003
49. Yuan D, Chen L, Xiong X et al (2016) Removal of uranium (VI) from aqueous solution by amidoxime functionalized superparamagnetic polymer microspheres prepared by a controlled radical polymerization in the presence of DPE. Chem Eng J 285:358–367. https://doi.org/10.1016/j.cej.2015.10.014